Talanta 225 (2021) 122022

Contents lists available at ScienceDirect

Talanta

journal homepage: www.elsevier.com/locate/talanta

Perfluorinated polymer modified vertical silicon nanowires as ultra low noise laser desorption ionization substrate for salivary metabolites profiling

Xinrong Jiang [a], Xiaoming Chen [a,c], Tao Wang [a], Yuexin Li [a], Aiwu Pan [b], Jianmin Wu [a,*]

[a] Institution of Analytical Chemistry, Department of Chemistry, Zhejiang University, Hangzhou, 310058, China
[b] Hospital of Zhejiang University, Hangzhou, 310058, China
[c] Well-healthcare Technologies Co., Hangzhou, 310051, China

ARTICLE INFO

Keywords:
Nanostructure-initiator mass spectrometry
Low background noise
Metabolomics
Saliva detection
Disease diagnosis

ABSTRACT

Metabolites in the body fluid are becoming a rich source of disease biomarkers. Developing an effective and high throughput detection and analysis platform of metabolites is of great importance for potential biomarker discovery and validation. Matrix-assisted laser desorption/ionization time-of-flight mass spectrometry (MALDI-TOF-MS) has been successfully applied in rapid biomolecules detection in large scale. However, non-negligible background interference in low molecule-weight region still constitutes a main challenge even though various nanomaterials have been developed as an alternative to traditional organic matrix. In this work, a novel composite chip, silicon nanowires loaded with fluorinated ethylene propylene (FEP@SiNWs) was fabricated. It can serve as an excellent substrate for nanostructure-initiator mass spectrometry (NIMS) detection with ultra-low background noise in low molecular weight region (<500 Da). Ion desorption efficiency and internal energy transfer of FEP@SiNWs were studied using benzylpyridinium salt and tetraphenylboron salt as thermometer chemicals. The results indicated that a non-thermal desorption mechanism might be involved in the LDI process on FEP@SiNWs. Owing to the higher LDI efficiency and low background interference of this novel substrate, the metabolic fingerprint of complex bio-fluids, such as human saliva, can be sensitively and stably acquired. As a proof of concept, FEP@SiNWs chip was successfully used in the detection of salivary metabolites. With the assistance of multivariate analysis, 22 metabolic candidates ($p < 0.05$) which can discriminate type 2 diabetes mellitus (2-DM) and healthy volunteers were found and identified. The role of these feature metabolites in the metabolic pathway involved in 2-DM was confirmed by literature mining. This work demonstrates that FEP@SiNWs-based NIMS might be served as an efficient and high throughput platform for metabolic biomarker exploration and clinical diagnosis.

1. Introduction

Matrix-assisted laser desorption/ionization time-of-flight mass spectrometry (MALDI-TOF-MS) has been widely applied in the detection and analysis of biomolecules [1]. The use of organic matrix contributes to laser energy absorption and analytes ionization [2–4]. However, the background interference from fragments of organic matrix in the low molecule-weight (LMW) region (<500 Da) cannot be ignored, thereby limiting the application of MALDI-TOF-MS in metabolic analysis [5,6]. In recent years, various inorganic candidates including graphene-based nanomaterials [7], carbon nanotubes [8], metal nanoparticles [9–12] and nanostructured silicon materials have been developed [13–16]. These nanomaterials show great advantages in laser energy absorption and ion desorption process because of the large surface area, good thermal confinement and charge transfer ability [11,17]. However, background signal originated from cluster of inorganic nanomaterials still cannot be eliminated in LMW range [18]. To overcome this problem, several works proposed that surface modification or coating suitable molecules on nanomaterials can significantly prevent the generation of background noise in LMW range [19,20]. One of the most effective strategies is to load initiators on porous silicon (pSi) which acts as a substrate to capture laser energy. After laser irradiation, the pSi

Abbreviations: PCA, principal component analysis; OPLS-DA, orthogonal partial least squares-discrimination analysis; APDMES, 3-aminopropyldimethylethoxysilane; $BisF_{17}$, bis(heptadecafluoro-1,1,2,2-tetrahydrodecyl) tetramethyldisiloxane.

* Corresponding author.
E-mail addresses: wjm-st1@zju.edu.cn, jmwu719@163.com (J. Wu).

https://doi.org/10.1016/j.talanta.2020.122022
Received 30 August 2020; Received in revised form 7 December 2020; Accepted 13 December 2020
Available online 17 December 2020

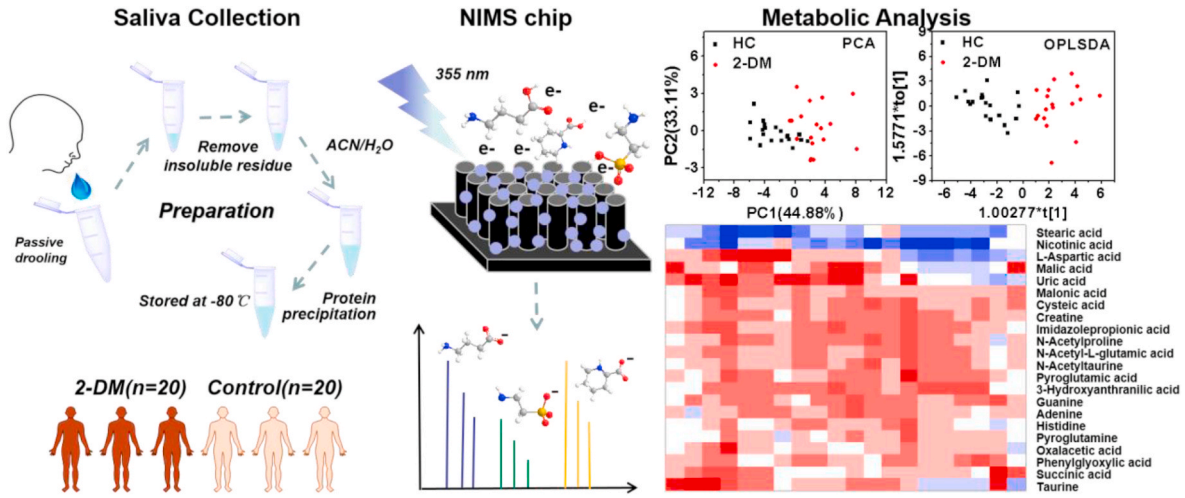

Fig. 1. Schematic workflow for the preparation and detection of saliva samples based on NIMS chip.

surface is heated and initiators trapped in Si clathrates can be released to promote the generation of intact molecular ions while producing lower silicon background signals [21]. This technique has been named as nanostructure-initiator mass spectrometry (NIMS) [20]. Usually, silane compounds containing amino groups like APDMES and perfluorinated compounds like $BisF_{17}$ were selected as initiators in negative or positive ionization mode, respectively [20,22,23]. Up to now, NIMS has been applied in tissue profiling, peptide and single cell analysis with high sensitivity and relatively low noise in LMW range. Using NIMS method, metabolic analysis in complex biological mixtures has been demonstrated [22–26]. However, non-negligible background signal from initiator fragments and substrates still could be found in LMW range when traditional NIMS materials were employed [18]. In addition, laser absorption efficiency and thermal confinement properties also play vital roles in the performance of NIMS approach. Therefore, attempt to seek more suitable NIMS substrates and initiators need to be achieved to further eliminate the background noise, so that metabolomics investigation on NIMS platform can be practically achieved [23].

Our previous work has demonstrated that vertical silicon nanowires (SiNWs) array has much higher laser absorption efficiency and better thermal confinement effect compared to pSi [27]. Accordingly, it only needs lower laser energy to desorb and ionize the analytes, thereby reducing extra background signal ionization [27]. In the present work, SiNWs array was firstly employed as NIMS substrate to host initiator to achieve a high signal to noise ratio in MS detection. In addition, perfluoroethylene propylene copolymer (FEP, CAS: 25067-11-2) was selected as a novel initiator owing to its low viscosity, low vapor pressure and non-hydrolysis properties, which meet the requirements for an ideal initiator [24]. By coating FEP preparation on vertical SiNWs array (FEP@SiNWs), a novel NIMS chip with ultra-low background interference in LMW range was obtained.

To demonstrate the feasibility of this novel NIMS substrate in metabolic analysis, human saliva samples were analyzed using FEP@SiNWs. Owing to the ultra-low background noise of the FEP@SiNWs chip, salivary metabolic profile can be reliably acquired on the NIMS platform in a high throughput way. With the assistance of statistical analysis, 22 metabolic candidates which can discriminate type 2 diabetes mellitus (2-DM) and healthy volunteers were selected and identified. Besides, the role of feature metabolites in 2-DM metabolic pathway was discussed in detail. We believe the NIMS platform established in this work can be pervasively applied in high throughput detection of metabolites in various biological samples.

2. Experimental section

2.1. Materials and reagents

Single-crystal silicon wafers (p type, <100>, 5–10 Ω cm) and silicon wafers (p type, <100>, 0.01–0.02 Ω cm) were purchased from Lijing Silicon Materials Co. (Quzhou, China). Hydrofluoric acid (HF, 40%), ethanol (EtOH) and acetonitrile (ACN) were purchased from Sinopharm Chemical Reagent Co. (Shanghai, China). Silver nitrate ($AgNO_3$), lauric acid (C12:0), palmitic acid (C16:0), stearic acid (C18:0), arachidic acid (C20:0), teracosanoic acid (C24:0), γ-aminobutyric acid, malonic acid, oxalacetic acid, valine, succinic acid, imidazolepropionic acid, glutamine, phenylglyoxylic acid, nicotinic acid, taurine, pyroglutamine, pyroglutamic acid, creatine, aspartic acid, malic acid, adenine, guanine, 3-hydroxyanthranilic acid, histidine, N-acetylproline, N-acetyltaurine, uric acid, cysteic acid, N-acetyl-L-glutamic acid and arginine standards were purchased from Aladdin Co. (Shanghai, China). Fluorinated ethylene propylene preparation (FEP preparation) was purchased from Jinhua Yonghe Fluorochemical Co. (Jinhua, China). 3-aminopropyldimethylethoxysilane (APDMES) was purchased from Meryer Co. (Shanghai, China).

Benzylpyridinium salt ($[BP]^+$) was synthesized from the reaction of pyridine (≥99.9%, Aladdin) and benzyl chloride (≥99.9%, Aladdin). Benzyl chloride was mixed with 1 mL pyridine at a molar ratio of 1:20 and heated in a water bath of 60 °C for 5 h. After the reaction, the excess pyridine was removed by vacuum evaporation. The synthetic product was redissolved in MeOH to prepare a 1 M $[BP]^+$ solution, which was diluted by 50% MeOH to obtain a working solution of 0.1 mM.

2.2. NIMS substrates fabrication

Vertical SiNWs array was fabricated via the one-step metal assisted chemical etching (MACE) method [27]. Briefly, the p-type silicon wafer (5–10 Ω cm) was cut to 3 cm × 3 cm, then chips were immersed in 0.02 M $AgNO_3$ and 4.8 M HF mixed solution for 15 min. After etching, Ag catalyst was removed with dilute nitric acid (HNO_3, 1:1 v/v). To guarantee that Ag catalyst was totally dissolved, the dilute HNO_3 washing time can't be less than 1 h.

Porous silicon was fabricated via the electrochemical etching procedure. In brief, the p-type silicon wafer (0.01–0.02 Ω cm) was cut to 3 cm × 3 cm and etched at 48 mA cm^{-2} for 30 min in Teflon cell. The etching solution was 25% HF diluted in EtOH.

For initiator loading, approximately 100 μL of FEP preparation or APDMES was added onto the SiNWs or porous silicon and soak the surface in initiator solution for 30 min, then the excess initiator was

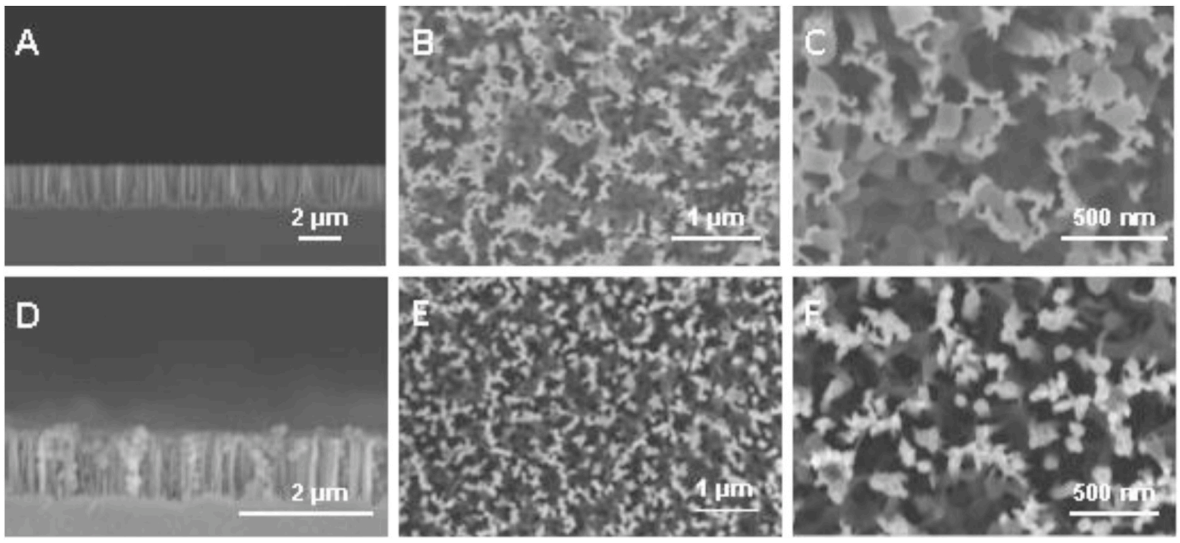

Fig. 2. Cross-section views of (A) SiNWs and (D) FEP@SiNWs. Top views of (B, C) FEP@SiNWs before laser irradiation and (E, F) FEP@SiNWs after irradiation. (C, F) are the magnified images of (B, E), respectively.

removed on spin coater to obtain uniform surface.

2.3. Procedure for salivary metabolites detection

A representative workflow for saliva sample detection is illustrated in Fig. 1, which include saliva sample collection, pretreatment, sample loading on NIMS chip, and mass spectrometric detection. In detail, saliva samples from 20 healthy volunteers and 20 patients diagnosed with 2-DM were collected in hospital of Zhejiang University between 8:30 a.m. and 10:30 a.m. The demographic information of 2-DM patients and healthy volunteers was provided in Table. S1 (ESI†). Before collection, all individuals were refrained from eating, drinking, smoking or oral cleaning procedure for at least 2 h. During the saliva collection procedure, all the donors were asked to lower head 45° down and keep silent for 5 min, then approximately 3 mL of unstimulated saliva was collected in 50 mL centrifuge tube through passive drooling. Next, the collected samples were centrifuged at 8000 g for 10 min at 4 °C to remove insoluble residues, then the resulting supernatant mixed with ACN and ultrapure water (1:1:1 v/v/v) to precipitate protein. The mixture was thoroughly vortexed for 10 min and centrifuged at 8000 g for 10 min at 4 °C. Finally, the supernatant was stored in refrigerator at −80 °C until use. The Ethical Committee of the Zhejiang University hospital approved the protocol and the methods were carried out in accordance with the approved guidelines.

After pipetting 2 μL of saliva sample onto substrate, the chips were stuck onto plate and then inserted into the instrument for detection. Mass spectra were obtained using the ultrafleXtreme MALDI-TOF/TOF instrument (Bruker Daltonics Co.). The instrument was equipped with a 355 nm Nd:YAG laser beam. The pulsed ion extraction was set at 120 ns and the laser parameter was set at 4_large. Final MS spectra were collected after adding 500 and 1000 times of laser shots for reflective and linear mode, respectively. All measurements were parallelly detected for three times. Since the absolute energy of this instrument is hard to measure directly, we use relative percentage of total energy to calculate laser energy. The relative laser energy can be adjusted by changing the value of global attenuator offset、attenuator offset and attenuator range as shown in the following equation:

$$E = \textit{Global attenuator offset} + \textit{Attenuator offset} + \textit{Attenuator range} \times \textit{percentage}$$

For the detection of benzylpyridinium salt, E was adjusted ranging from 55% to 71% in linear positive mode; For the detection of real saliva samples or analytes, E was set at 57% in reflective negative mode.

2.4. Identification of the metabolites in saliva

The metabolites detected in saliva were identified using MALDI-TOF/TOF tandem mass spectrometry and UPLC-MS/MS. In detail, metabolites were firstly identified by searching Human Metabolome Database (http://www.hmdb.ca/) using exact molecular weights (MS1-level) and main fragment peaks m/z (MS/MS) obtained from UPLC-MS/MS. Then commercial standard reagents were employed to verify the identified metabolites by comparing the exact mass and fragment profile derived from saliva samples and standard sample on MALDI-TOF/TOF tandem mass spectrometry. The detailed experimental parameters of UPLC-MS analysis were provided in ESI†.

2.5. Data handling and statistical analysis

The mass spectra were analyzed to find potential biomarker candidates to discriminate between 2-DM patients and healthy volunteers. Mass spectra acquisition and processing were performed by FlexAnalysis (Bruker Daltonics Co.). ClinproTool (Bruker Daltonics Co.) was utilized for peak finding (S/N > 3). The mass spectra of each real saliva sample were normalized in MATLAB and then performed t-test to find feature peaks ($p < 0.05$). Here, we investigated two kinds of normalization methods, including normalization to intensity of the highest peak and normalization to MS "total useful signal" (MSTUs). MSTUs uses the total intensity of peaks that are present in all samples under study as the normalization factor [28]. Unsupervised PCA was achieved in MATLAB using the selected feature peaks and supervised OPLS-DA was performed by importing feature peak data including group information into SIMCA software. R^2X, R^2Y and Q^2 act as a mirror reflecting the predictive credibility of the model. Perturbations of significantly differential metabolites in 2-DM patients were expressed as a fold-change pattern (Log2) by calculating the ratio of 2-DM's relative intensity to the average value of health control ($n = 20$). To uncover the globally disturbed metabolic pathways in 2-DM patients, pathway analysis was realized based on the selected metabolites using MetaboAnalyst.

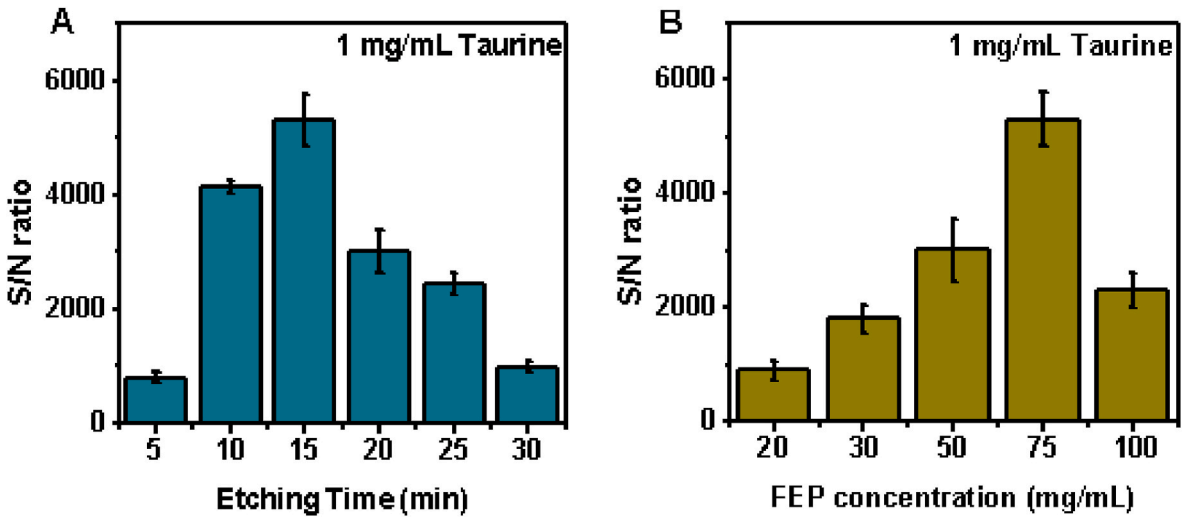

Fig. 3. The S/N ratio of taurine at different etching time or different FEP concentration. (A) Etching process was varied from 5 to 30 min. (B) The FEP concentration was varied from 20 to 100 mg mL^{-1} with fixed etching time.

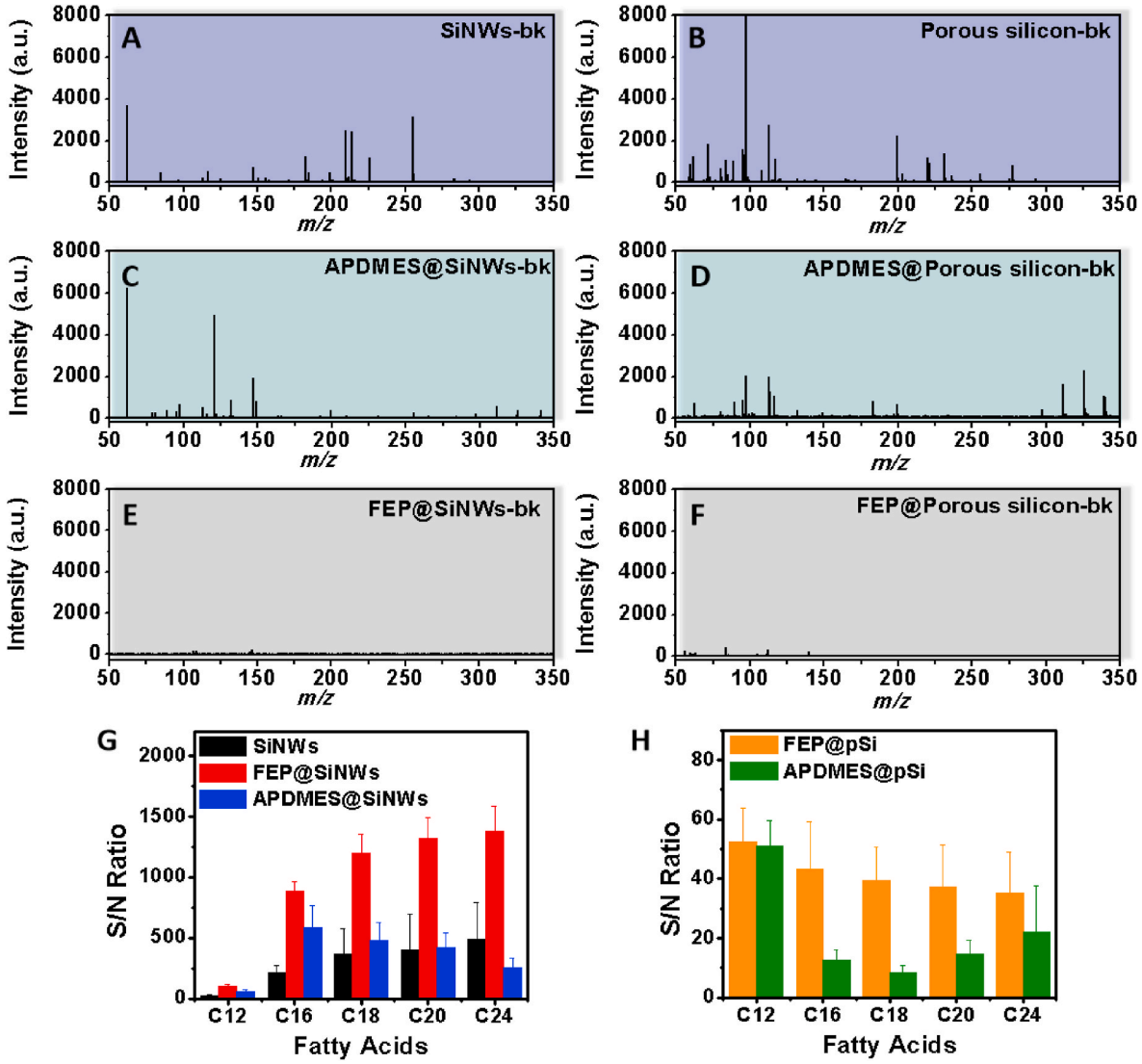

Fig. 4. The analytical performances of various substrates were compared in terms of background noise and standard fatty acids detection. (A)–(F) presented the background noise of different substrates in LWM region. (G) S/N ratio of standard fatty acids on SiNWs, FEP@SiNWs and APDMES@SiNWs substrate. (H) S/N ratio of standard fatty acids on FEP@pSi and APDMES@pSi substrate.

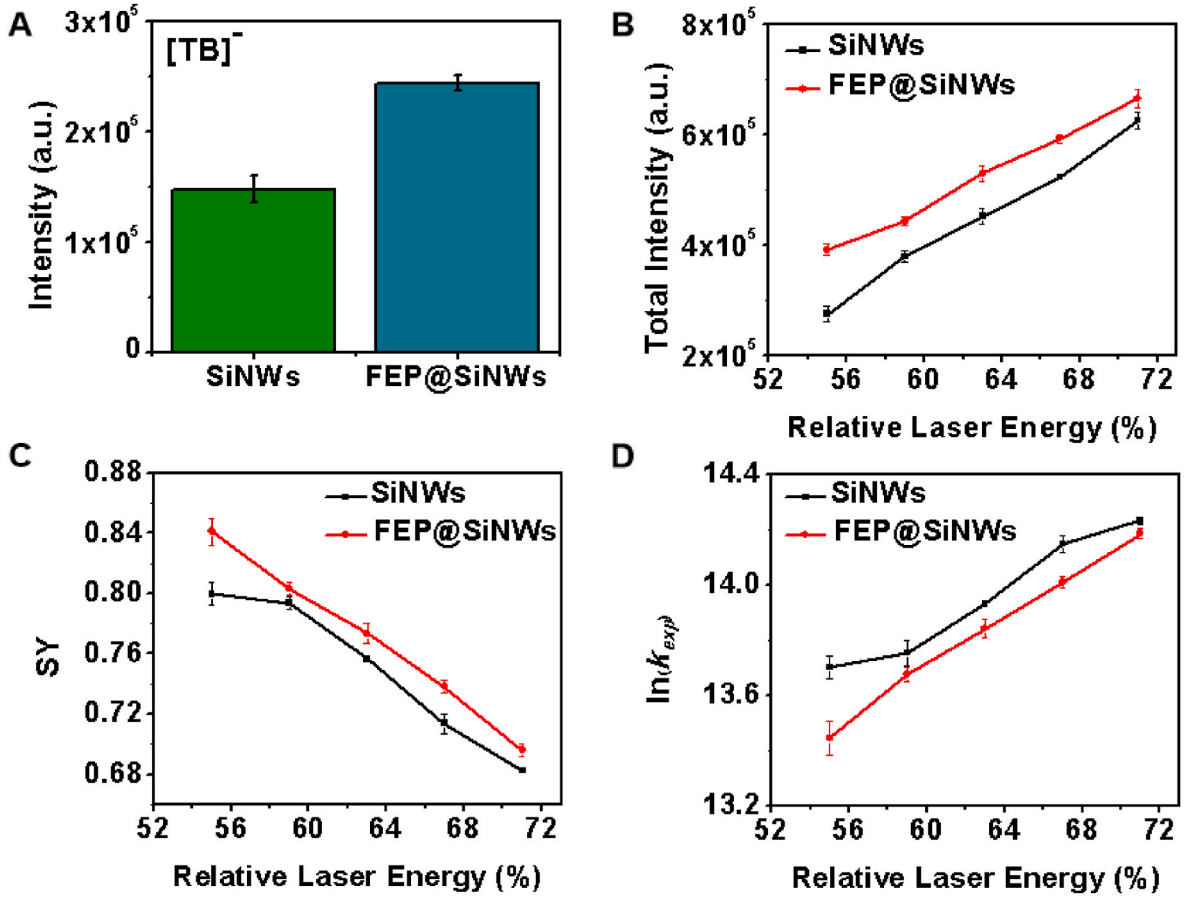

Fig. 5. The Determination of Ion-Desorption Efficiency and Internal Energy Transfer in the LDI process of FEP@SiNWs and SiNWs substrates at different laser energy. (A) The total intensity of TB ions desorbed from FEP@SiNWs and SiNWs substrates. (B) The total intensity of BP ions desorbed from FEP@SiNWs and SiNWs substrates. (C) The survival yield of BP ions. (D) The ln (k_{exp}) of BP ions, ln (k_{exp}) is positively related to average internal energy.

3. Results and discussion

3.1. Characterization of SiNWs and FEP@SiNWs substrate

The morphologies of the as-prepared SiNWs and FEP@SiNWs substrate were characterized by scanning electron microscopy (SEM) and the surface chemistry of the two samples was investigated by the X-ray photoelectron spectroscopy (XPS), respectively. According to the cross-section views of the SEM results, both SiNWs and FEP@SiNWs substrates displayed a well-aligned and vertical array structure (Fig. 2). After loading initiator, it can be clearly observed that FEP polymer particles have been successfully loaded onto the SiNWs (Fig. 2B–D). Besides, the amount of FEP polymer particles sharply decreased after UV laser irradiation (Fig. 2E and F). From the survey spectra and detail spectra of XPS (Fig. S1, ESI†), the freshly etched SiNWs sample shows Si 2p, Si 2s, and a low-intensity C 1s peak, which is mainly due to adventitious carbon contamination. The Si 2p peak was observed at about 103.1 eV due to the oxidation of SiNWs by HNO_3 in the process of washing out Ag catalyst. For FEP@SiNWs, an obvious C 1s peak at 286.4 eV and a high-intensity of F 1s peak at 685.7 eV were observed on the modified surface. The line positions of O 1s and Si 2p peak displayed no change compared to SiNWs, thereby verifying the successful physical adsorption of FEP onto SiNWs surface.

3.2. Optimization of FEP@SiNWs performance

To obtain a highly efficient NIMS substrate, the experimental parameters for preparation of FEP@SiNWs chip were optimized by adjusting time for etching SiNWs and initiator concentration. NIMS performance was evaluated by standard taurine solution (1 mg mL^{-1}) under different experimental condition. The duration of the etching process was varied from 5 to 30 min, and FEP concentration was varied from 20 mg mL^{-1} to 100 mg mL^{-1}. The results indicated that the highest S/N ratio was obtained at the sample etched with the 15 min and loaded with 75 mg mL^{-1} of FEP (Fig. 3). It should be mentioned that NIMS performance would decrease if high amount of FEP was applied onto SiNWs. Because NIMS efficiency depends on absorption of laser energy by the SiNWs substrate, applying excess initiator may reduce the laser intensity at the silicon surface and consequently reduces the overall energy received on the NIMS substrate.

3.3. Background reduction and signal enhancement effect of FEP@SiNWs for MALDI-TOF MS detection

The appearance of background ions in laser desorption ionization (LDI) mass spectrometry was owing to the restructuring of nanostructured silicon and formation of surface ion [18,29]. The presence of initiator coating on the nanostructured silicon can significantly inhibit the generation of surface ions upon laser irradiation, because initiator can help transfer laser energy to sample molecules but rarely ionize, thereby generating mass spectra with lower background noise [18]. The type of initiator and hosting substrate play vital roles in reducing background noise in LMW region and improving S/N ratio for metabolites detection. To evaluate the NIMS efficiency, a mixed solution of standard fatty acids (C12:0, C16:0, C18:0, C20:0, C24:0) was employed to compare the performance of different NIMS substrate. For bare pSi and SiNWs, high background signal derived from cluster of silicon ions was observed in both substrate (Fig. 4A and B). Usually, APDMES has

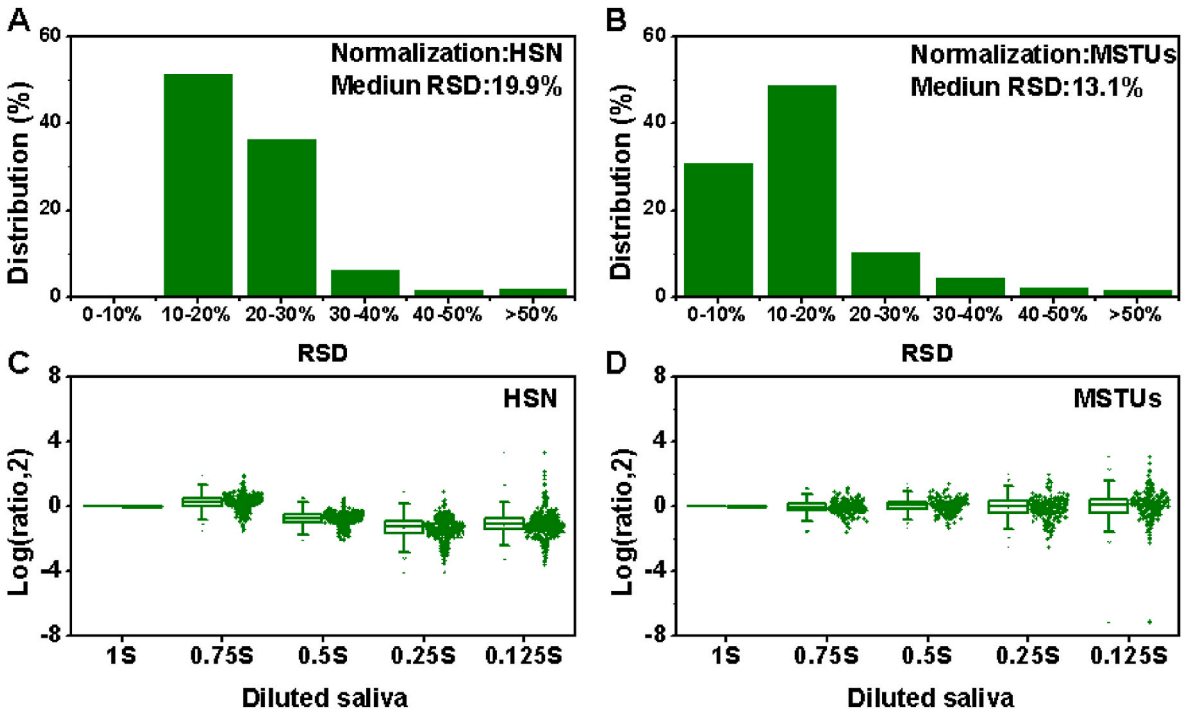

Fig. 6. (A, B) Distribution of relative standard deviation (RSD) of the signal intensities of peaks (S/N > 3) after different normalization methods. (C, D) The diluted saliva sample peak ratio distributions were presented using box plots after different normalization methods.

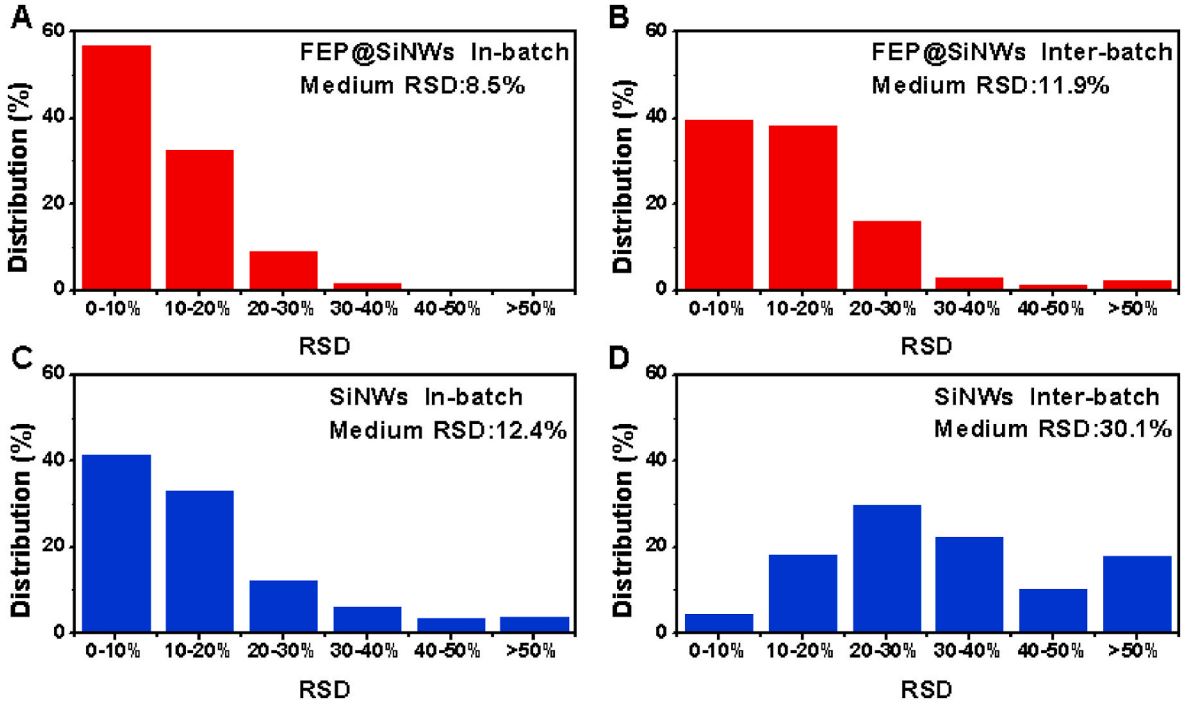

Fig. 7. Distribution of RSD of the signal intensities within the same batch (A, C) or between different batches (B, D) of FEP@SiNWs or SiNWs substrates after normalized by MSTUs. Inter-batch stability was calculated after normalization using the average intensities of different batches.

been regarded as the most effective initiator in negative mode [23]. However, after coating APDMES on pSi or SiNWs substrate, the background signal can be still found even though the number of background signals significantly decreased (Fig. 4C and D). In contrast, FEP@pSi and FEP@SiNWs displayed ultra-low background noise in LMW range (Fig. 4E and F), indicating that FEP is an ideal initiator in NIMS technology owing to its low viscosity, low vapor pressure and non-hydrolysis properties. In addition, the S/N ratio of standard fatty acids detected on FEP@SiNWs is significantly larger than that on FEP@pSi (Fig. 4G and H), because the SiNWs have much higher laser absorption efficiency and better thermal confinement compared to pSi, as indicated in our previous work [27].

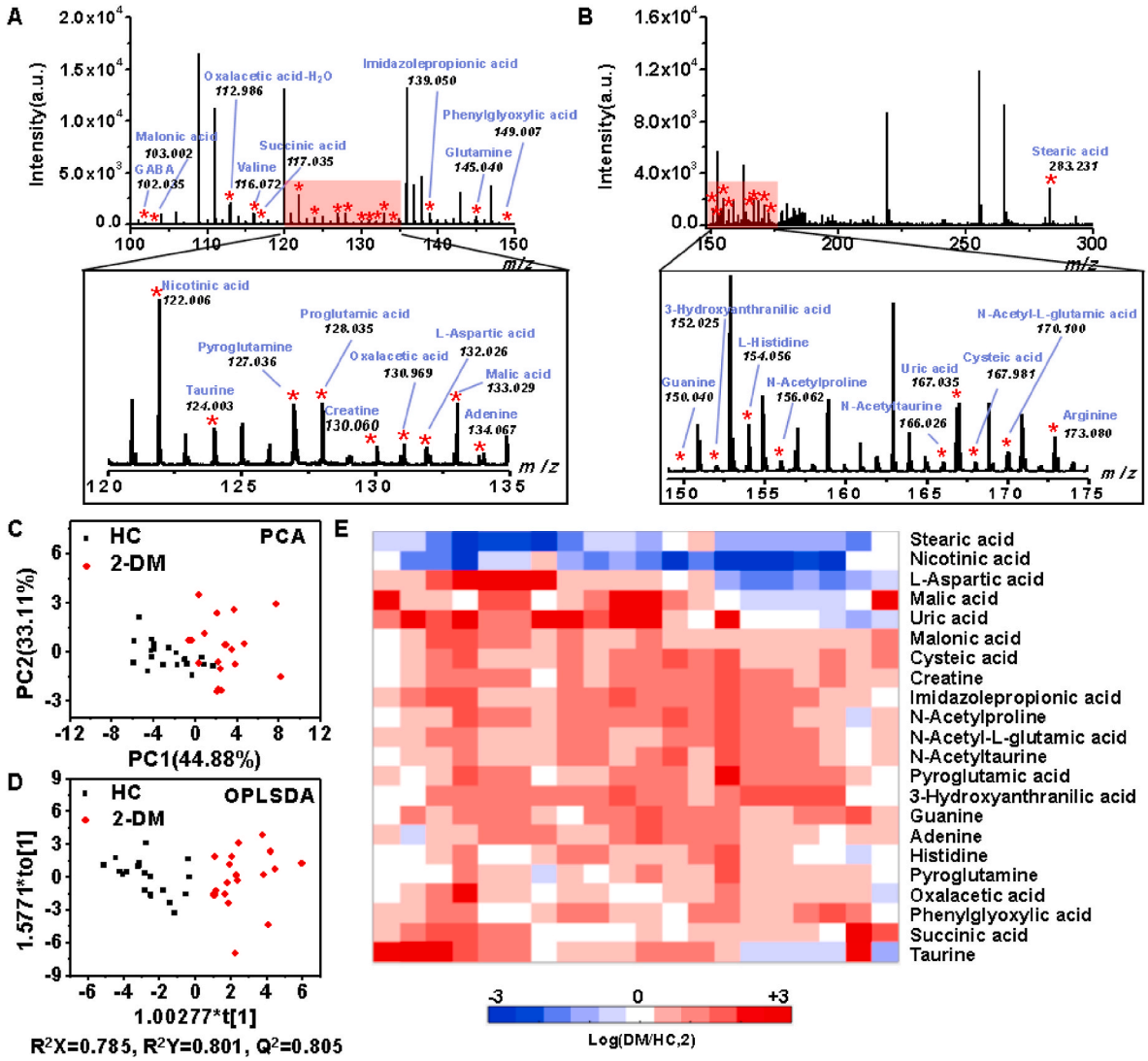

Fig. 8. (A, B) LDI mass spectra of saliva metabolite extract using FEP@SiNWs substrate. (A) m/z: 100–150 Da. (B) m/z: 150–300 Da. (C, D) Discrimination results among saliva samples including 2-DM (red, n = 20) and health (black, n = 20) groups. Unsupervised PCA and supervised OPLSDA was based on 22 selected peaks after normalization. (E) Changes in the relative intensity values of potential biomarker candidates in 2-DM patients. The ratio values were expressed as a fold-change pattern (Log2) by calculating the ratio of 2-DM's relative intensity to average value of health control (n = 20). Each column represents a sample, and the data used was the average of three replicates for each saliva sample.

3.4. Determination of ion-desorption efficiency and internal energy transfer

To further investigate whether thermal-driven or phase-transition-driven desorption process dominants the overall LDI process, ion desorption efficiency and internal energy transfer of FEP@SiNWs were probed and correlated using benzylpyridinium salt $[BP]^+$ and tetraphenylboron salt $[TB]^-$ as the chemical thermometer [11,30,31]. The detailed definition and calculation of desorption efficiency, survive yield (SY), dissociation rate coefficients (k_{exp}) and average internal energy are provided in ESI†. The desorption efficiency, SY and ln (k_{exp}) of SiNWs and FEP@SiNWs were plotted against different UV laser energy, ln (k_{exp}) is positively related to average internal energy. Compared with the behavior on bare SiNWs, both $[BP]^+$ and $[TB]^-$ exhibit higher total intensity on FEP@SiNWs substrate (Fig. 5A and B), indicating the higher ion desorption efficiency of FEP@SiNWs chip in both positive and negative ion modes. However, the total ion intensity of $[BP]^+$ (FEP@SiNWs > SiNWs) and ln (k_{exp}) (FEP@SiNWs < SiNWs) show an opposite trend (Fig. 5B–D). This phenomenon can't be solely explained by thermal desorption mechanism, inferring that a non-thermal desorption mechanism might be involved in the LDI process. As shown in Fig. 2, the amount of FEP polymer particles loaded onto SiNWs sharply decreased after UV laser irradiation (Fig. 2C, F), indicating that phase transition of polymer particles could be involved in the desorption/ionization process. Based on the above findings, we can conclude that non-thermal desorption plays a significant role in the overall LDI process on FEP@SiNWs substrate, and the phase transition of FEP particles might contribute to higher ion desorption efficiency.

3.5. Comparing different normalization methods for acquiring salivary metabolites profiles

Saliva volume and solute concentration are greatly affected by water consumption, diet and excretion. To minimize the impact of these factors on downstream analysis, a standard sample collection as described in experimental section should be strictly followed. In addition, normalization procedures after acquiring metabolic profiles are also required. Two kinds of normalization methods including normalization to intensity of the highest peak signal (HSN) and normalization to MS "total useful signal" (MSTUs) were investigated in this study. The

Table 1
Summary of p values of feature peaks that could be used to distinguish 2-DM patients from control subjects.

No.	Detected m/z	Metabolites	p value	Trend
1	167.981	Cysteic acid	2.63×10^{-6}	↑
2	150.021	Guanine	5.06×10^{-6}	↑
3	130.060	Creatine	7.05×10^{-6}	↑
4	170.100	N-Acetyl-L-glutamic acid	1.52×10^{-5}	↑
5	139.035	Imidazolepropionic acid	1.62×10^{-5}	↑
6	152.025	3-Hydroxyanthranilic acid	2.37×10^{-5}	↑
7	156.062	N-Acetylproline	2.69×10^{-5}	↑
8	166.026	N-Acetyltaurine	6.24×10^{-5}	↑
9	149.007	Phenylglyoxylic acid	6.29×10^{-5}	↑
10	103.002	Malonic acid	7.45×10^{-5}	↑
11	134.067	Adenine	2.88×10^{-4}	↑
12	167.035	Uric acid	4.39×10^{-4}	↑
13	128.035	Pyroglutamic acid	6.05×10^{-4}	↑
14	133.029	Malic acid	3.23×10^{-3}	↑
15	283.231	Stearic acid	5.26×10^{-3}	↓
16	127.036	Pyroglutamine	6.76×10^{-3}	↑
17	132.026	L-Aspartic acid	8.48×10^{-3}	↑
18	124.003	Taurine	9.23×10^{-3}	↑
19	122.006	Nicotinic acid	1.27×10^{-2}	↓
20	154.056	L-Histidine	1.74×10^{-2}	↑
21	130.969	Oxalacetic acid	3.91×10^{-2}	↑
22	117.035	Succinic acid	4.76×10^{-2}	↑

variance between replicated measurements and the correction effect to saliva dilution were combined to evaluate the performance of the different normalization methods. Here, a model saliva sample (1S) was prepared by mixing all collected saliva samples in equal volumes and a series of diluted saliva (0.75S, 0.5S, 0.25S, 0.125S) was prepared with water at different dilution ratios. The correction effects of normalization to saliva dilution were presented in a box-plot by calculating the peak ratios between diluted samples and original sample after normalization. The log ratios between the diluted saliva sample and 1S sample should be close to 0 for most metabolites under the reasonable assumption that there are little biological variations during the dilution process. To calculate the variance between replicated measurements, three different batches of optimized FEP@SiNWs were prepared, three FEP@SiNWs chips were applied in each batch and triplicates were done on each chip. Finally, 27 spectra were obtained and used for statistical analysis. Fig. 6 indicated that normalization using MSTUs method is better than HSN for salivary metabolomic applications.

3.6. In-batch and inter-batch stability of FEP@SiNWs chip

Additionally, we examined the stability of in-batch and inter-batch detection to confirm the repeatability of FEP@SiNWs in MS signal (Fig. 7A and B). The model saliva sample was spotted on the FEP@SiNWs substrate for non-targeted metabolic fingerprint analysis. After normalization with MSTUs, all peaks (S/N > 3) were utilized to measure the variations in-batch and inter-batch detection. As shown in Fig. 7, FEP@SiNWs displayed more excellent intra-batch (medium RSD = 8.5%) and inter-batch stability (medium RSD = 11.9%) than that on SiNWs owing to the significantly lower background noise. The small variation of in-batch and inter-batch detection on FEP@SiNWs guaranteed the reliability of collective data.

3.7. Salivary metabolic analysis of 2-DM and healthy control

Saliva is an ideal biological sample because it is collected non-invasively and the risk of acquired infections is minimal [32]. The concentrations of endogenous metabolites in saliva directly reflect the metabolic status of human body, and further indicate whether human body suffers from metabolic diseases such as cancer, diabetes, gout, periodontal diseases and so on [32–36]. Therefore, saliva may serve as an excellent biofluid for disease diagnosis. 2-DM is a complex and systematic disease caused by genetic and environmental factors. Nowadays, the most common diagnostic methods for 2-DM are fasting plasma glucose (FPG) test, oral glucose tolerance test, and glycated test [37]. However, since the early symptoms of 2-DM are not obvious, it is necessary to develop a non-invasive screening technique that can be widely and persistently applied in personal healthcare.

In the present work, saliva samples from 20 healthy volunteers and 20 2-DM patients were collected and analyzed for non-targeted metabolic analysis, the representative MALDI-TOF mass spectra of saliva samples in the metabolic fingerprint region were provided (Fig. S2, ESI†). Using the FEP@SiNWs chip, the MS spectra of small molecules like amino acids and fatty acids in saliva can be unambiguously detected (Fig. 8A and B). Combining UPLC-MS/MS and MALDI-TOF/TOF tandem mass spectrometry, the metabolites detected in saliva were identified (Table. S2-4, ESI†). Through two-sided t-test by MATLAB software, setting p value < 0.05, 22 metabolites were selected as potential candidates for distinguishing 2-DM patients from healthy volunteers (Table 1). To validate whether the selected feature metabolites can discriminate the 2-DM patients from the healthy control people, supervised OPLS-DA or unsupervised PCA was employed. The results indicated that the 2-DM and healthy control can be successfully discriminated using the selected 22 metabolites found in saliva (Fig. 8C and D). Meanwhile, box plots were performed to display the perturbations of feature metabolites in 2-DM group (Figs. 8E and 9). The results show that adenine, guanine, aspartic acid, creatine, cysteic acid, histidine, 3-hydroxyanthranilic acid, malic acid, imidazolepropionic acid, malonic acid, N-Acetyl-L-glutamic acid, N-Acetylproline, N-Acetyltaurine, oxalacetic acid, phenylglyoxylic acid, pyroglutamic acid, pyroglutamine, succinic acid, taurine and uric acid are up-regulated in 2-DM patients whereas stearic acid and nicotinic acid are down-regulated. The increase in the relative concentration of malic acid, oxalacetic acid and succinic acid was significantly correlated with the 2-DM phenotype and indicated an elevated activity of TCA cycle flux [38–41]. Previous studies have indicated an augmented purine metabolism in 2-DM subjects and associated increase in serum uric acid levels and urinary purine metabolites levels, this phenomenon revealed an adaptive mechanism that provides energy for cellular metabolic activities when the glucose oxidation is not adequate [42,43]. Serum analysis of Chinese hamsters with 2-DM also revealed that the level of stearic acid was slightly decreased [38]. Up-regulation of taurine was observed in urinary metabolomics of both 2-DM human and rodent models. The increased excretion of taurine may arise from altered renal reabsorption of taurine as a result of reduced GFR or possibly as a general stress response, particularly following damage to the liver [44]. In urine samples of 2-DM subjects, aspartic acid and histidine were also found to be excreted at significantly higher levels than in urine samples of the healthy group [45]. Besides, imidazolepropionic acid is a product of histidine metabolism which may involve oxidation or transamination, and the increase might be directly related to the accumulation of histidine. 3-Hydroxyanthranilic acid is an intermediate in the metabolism of tryptophan, and its increase may be correlated to the elevated tryptophan level [38,46]. N-Acetyl-L-glutamic acid is biosynthesized from glutamic acid and acetyl-CoA by the enzyme N-acetylglutamate synthase (NAGS), and glutamic acid is reported to be upregulated in 2-DM subjects [46,47]. Besides, the increase of N-Acetylproline and N-Acetyltaurine could be explained by the accumulation of proline and taurine observed in 2-DM models [44,48]. Untargeted serum metabolic profiling also revealed the higher malonic acid level in 2-DM patients, this phenomenon might be explained by the altered nucleotide metabolism [41]. The abnormal creatine level was also observed in 2-DM plasma metabolomics, which directly reflected the altered creatine metabolism [49,50]. Pyroglutamic acid and pyroglutamine were involved in glutathione metabolism, their increase may be related to the higher concentration of their precursors which have been observed in 2-DM model [47,51]. Although the majority of these candidate biomarkers were implicated to known diabetic processes, several biomarkers (cysteic acid, phenylglyoxylic acid and

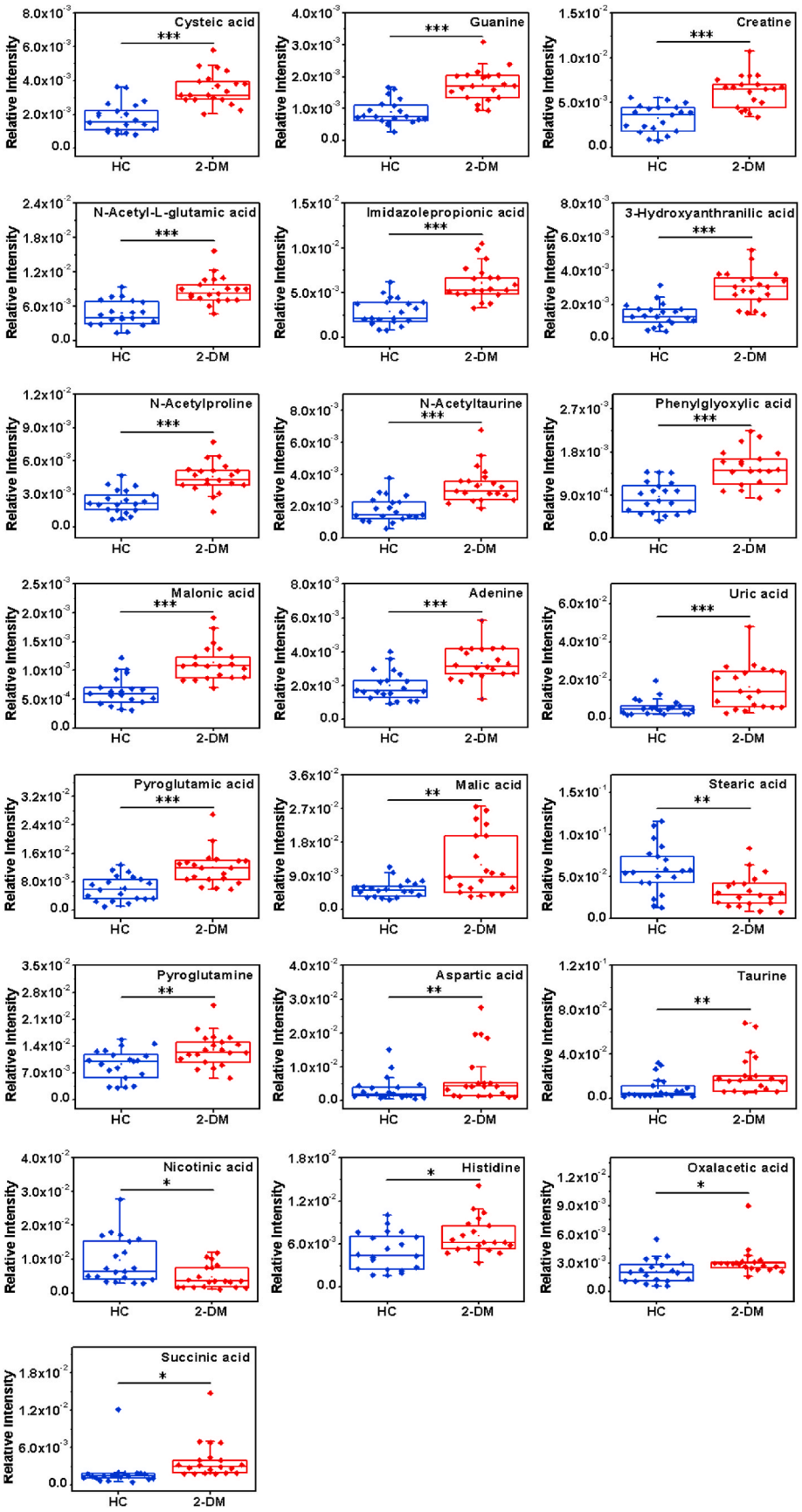

Fig. 9. Box plots of the levels of potential metabolic markers that could be used to distinguish 2-DM patients from control subjects. * represents $p < 0.05$, ** represents $p < 0.01$ and *** represents $p < 0.001$.

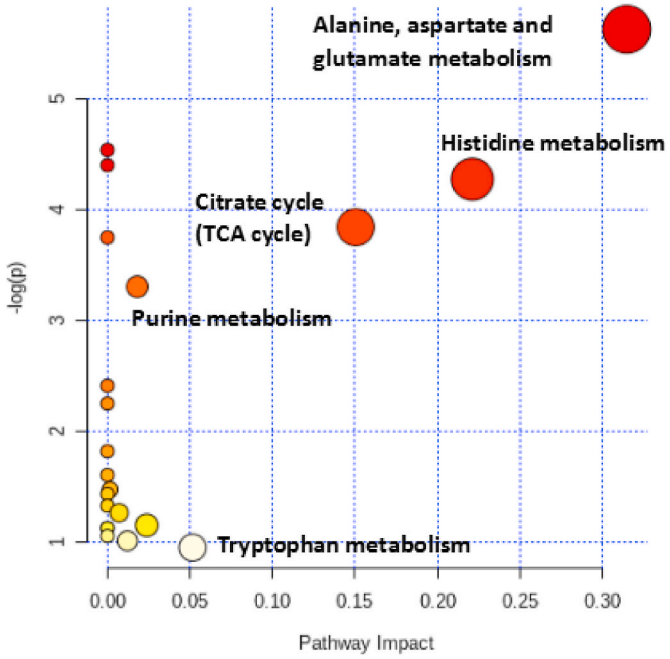

Fig. 10. The impact pathway analysis of 2-DM related metabolites based on MetaboAnalyst.

nicotinic acid) have not previously been suggested as possible biomarkers for diabetes. Meanwhile, the relevant metabolic pathways of the potential differential metabolites were provided through searches of HMDB (Table. S5, ESI†). The impact pathway analysis of 2-DM related metabolites using MetaboAnalyst also confirm the correlation between the selected metabolites and 2-DM disease (Fig. 10).

4. Conclusion

In summary, we developed a novel NIMS chip, FEP@SiNWs as an effective substrate for rapid salivary metabolic analysis with little background interference. The phase transition of initiator on the NIMS substrate was proved by SEM and the contribution of FEP to improvement of desorption efficiency was confirmed using $[BP]^+$ and $[TB]^-$ as model molecules. We demonstrated that salivary metabolic analysis can be reliably performed on the FEP@SiNWs chip because of its lower background noise, high signal to noise ratio and good repeatability. With this newly developed NIMS platform, non-targeted metabolic analysis for saliva samples from 2-DM patients and healthy volunteers could be reliably analyzed in a high throughput way. With the assistance of statistical analysis, 22 biomarker candidates with the capability to discriminate 2-DM patients from healthy volunteers were sorted out and identified. This work may contribute to rapid non-invasive clinical diagnosis in large scale and health management. Our ongoing work has further indicated that metabolomics-based non-invasive screening of malignant tumor can also be achieved on this platform.

Credit author statement

Xinrong Jiang: Conceptualization, Methodology, Investigation, Data curation, Software, Formal analysis, Writing – original draft, Xiaoming Chen: Software, Visualization, Validation, Writing- Reviewing and Editing. Tao Wang: Visualization, Writing- Reviewing and Editing. Yuexin Li: Visualization, Writing- Reviewing and Editing, Aiwu Pan: Sample collection, Clinical information collation, Jianmin Wu: Conceptualization, Resources, Funding acquisition, Writing- Reviewing and Editing, Supervision, Project administration.

Declaration of competing interest

The authors declare that they have no known competing financial interests or personal relationships that could have appeared to influence the work reported in this paper.

Acknowledgements

This study is supported by grants from the National Natural Science Foundation of China [grants number 21874118, 21575127].

Appendix A. Supplementary data

Supplementary data to this article can be found online at https://doi.org/10.1016/j.talanta.2020.122022.

References

[1] J. Hajduk, J. Matysiak, Z.J. Kokot, Clin. Chim. Acta 458 (2016) 84.
[2] G. Groeneveld, M. de Puit, S. Bleay, R. Bradshaw, S. Francese, Sci. Rep. 5 (2015) 11716.
[3] J. Hu, F. Liu, H. Ju, Angew Chem. Int. Ed. Engl. 55 (2016) 6667.
[4] M.A. Rodrigo, O. Zitka, S. Krizkova, A. Moulick, V. Adam, R. Kizek, J. Pharmaceut. Biomed. Anal. 95 (2014) 245.
[5] B. Fuchs, R. Suss, J. Schiller, Prog. Lipid Res. 50 (2011) 132.
[6] P.J. Trim, M.F. Snel, Methods 104 (2016) 127.
[7] M. Lu, Y. Lai, G. Chen, Z. Cai, Anal. Chem. 83 (2011) 3161.
[8] C.Y. Shi, C.H. Deng, Analyst 141 (2016) 2816.
[9] Y.H. Cheng, Y. Zhang, S.L. Chau, S.K. Lai, H.W. Tang, K.M. Ng, ACS Appl. Mater. Interfaces 8 (2016) 29668.
[10] J. Sekula, J. Niziol, W. Rode, T. Ruman, Anal. Chim. Acta 875 (2015) 61.
[11] K. Ng, S. Chau, H. Tang, X. Wei, K. Lau, F. Ye, A.M. Ng, J. Phys. Chem. C 119 (2015) 23708.
[12] W.J. Chiu, T.K. Ling, H.P. Chiang, H.J. Lin, C.C. Huang, ACS Appl. Mater. Interfaces 7 (2015) 8622.
[13] M. Dupre, C. Enjalbal, S. Cantel, J. Martinez, N. Megouda, T. Hadjersi, R. Boukherroub, Y. Coffinier, Anal. Chem. 84 (2012) 10637.
[14] A.R. Korte, S.A. Stopka, N. Morris, T. Razunguzwa, A. Vertes, Anal. Chem. 88 (2016) 8989.
[15] W.G. Lewis, Z. Shen, M.G. Finn, G. Siuzdak, Int. J. Mass Spectrom. 226 (2003) 107.
[16] J. Gao, M. de Raad, B.P. Bowen, R.N. Zuckermann, T.R. Northen, Anal. Chem. 88 (2016) 1625.
[17] E.P. Go, J.V. Apon, G. Luo, A. Saghatelian, R.H. Daniels, V. Sahi, R. Dubrow, B. F. Cravatt, A. Vertes, G. Siuzdak, Anal. Chem. 77 (2005) 1641.
[18] T. Guinan, M. Ronci, R. Vasani, H. Kobus, N.H. Voelcker, Talanta 132 (2015) 494.
[19] S. Alexandra Iakab, P. Rafols, M. Garcia-Altares, O. Yanes, X. Correig, Adv. Funct. Mater. 29 (2019).
[20] T.R. Northen, O. Yanes, M.T. Northen, D. Marrinucci, W. Uritboonthai, J. Apon, S. L. Golledge, A. Nordstrom, G. Siuzdak, Nature 449 (2007) 1033.
[21] T.N. Moening, V.L. Brown, L. He, ANAL METHODS-UK 8 (2016) 8234.
[22] H.K. Woo, T.R. Northen, O. Yanes, G. Siuzdak, Nat. Protoc. 3 (2008) 1341.
[23] A. Amantonico, L. Flamigni, R. Glaus, R. Zenobi, Metabolomics 5 (2009) 346.
[24] R. Calavia, F.E. Annanouch, X. Correig, O. Yanes, J PROTEOMICS 75 (2012) 5061.
[25] J. Li, R.H. Lipson, Anal. Chem. 85 (2013) 6860.
[26] G.J. Patti, H.K. Woo, O. Yanes, L. Shriver, D. Thomas, W. Uritboonthai, J.V. Apon, R. Steenwyk, M. Manchester, G. Siuzdak, Anal. Chem. 82 (2010) 121.
[27] X. Chen, T. Wang, L. Lin, F. Wo, Y. Liu, X. Liang, H. Ye, J. Wu, ACS Appl. Mater. Interfaces 10 (2018) 14389.
[28] J.J. Mikkonen, S.P. Singh, M. Herrala, R. Lappalainen, S. Myllymaa, A.M. Kullaa, J. Periodontal. Res. 51 (2016) 431.
[29] L.R. de Oliveira, C. Martins, T.K. Fidalgo, L.B. Freitas-Fernandes, T.R. de Oliveira, A.L. Soares, F.C. Almeida, A.P. Valente, I.P. de Souza, J. Proteome Res. 15 (2016) 2491.
[30] Z.T. Dame, F. Aziat, R. Mandal, R. Krishnamurthy, S. Bouatra, S. Borzouie, A. C. Guo, T. Sajed, L. Deng, H. Lin, P. Liu, E. Dong, D.S. Wishart, Metabolomics 11 (2015) 1864.
[31] D.C. Mueller, M. Piller, R. Niessner, M. Scherer, G. Scherer, J. Proteome Res. 13 (2014) 1602.
[32] J. Wei, G. Xie, Z. Zhou, P. Shi, Y. Qiu, X. Zheng, T. Chen, M. Su, A. Zhao, W. Jia, INT J CANCER 129 (2011) 2207.
[33] A. Menke, S. Casagrande, C.C. Cowie, Ann. Epidemiol. 28 (2018) 681.
[34] B.M. Warrack, S. Hnatyshyn, K.H. Ott, M.D. Reily, M. Sanders, H. Zhang, D. M. Drexler, J Chromatogr B Analyt Technol Biomed Life Sci 877 (2009) 547.
[35] T.R. Northen, H.K. Woo, M.T. Northen, A. Nordstrom, W. Uritboonthail, K. L. Turner, G. Siuzdak, J. Am. Soc. Mass Spectrom. 18 (2007) 1945.
[36] Y. Li, X. Cao, L. Zhan, J. Xue, J. Wang, C. Xiong, Z. Nie, Chem Commun (Camb) 54 (2018) 10905.
[37] H.W. Tang, K.M. Ng, W. Lu, C.M. Che, Anal. Chem. 81 (2009) 4720.
[38] C. Wang, J. Yu, R. Zhang, W. Wang, Z. Shi, Y. Liu, G. Song, H. Wang, N. Han, L. Huang, Y. An, S. Tian, Z. Chen, J PROTEOMICS 223 (2020) 103823.

[39] B.M. Abu, M.R. Sarmidi, K.K. Cheng, K.A. Ali, C.L. Suan, H.H. Zaman, H. Yaakob, Mol. Biosyst. 11 (2015) 1742.
[40] Y. Zeng, A. Mtintsilana, J.H. Goedecke, L.K. Micklesfield, T. Olsson, E. Chorell, Metabolism 95 (2019) 57.
[41] H. Wang, H. Zhang, L. Yao, L. Cui, L. Zhang, B. Gao, W. Liu, D. Wu, M. Chen, X. Li, A. Ji, Y. Li, Clin. Chim. Acta 477 (2018) 39.
[42] Y. Tanaka, I. Hisatome, T. Kinugawa, H. Tanaka, Y. Tomikura, F. Ando, T. Matsuura, G. Igawa, K. Matsubara, Y. Yamamoto, M. Yamawaki, R. Yamamoto, K. Ogino, O. Igawa, T. Ikeda, C. Shigemasa, A. Takeda, Intern Med 42 (2003) 788.
[43] N. Gogna, M. Krishna, A.M. Oommen, K. Dorai, Mol. Biosyst. 11 (2015) 595.
[44] R.M. Salek, M.L. Maguire, E. Bentley, D.V. Rubtsov, T. Hough, M. Cheeseman, D. Nunez, B.C. Sweatman, J.N. Haselden, R.D. Cox, S.C. Connor, J.L. Griffin, PHYSIOL GENOMICS 29 (2007) 99.
[45] C.J. Chen, W.L. Liao, C.T. Chang, Y.N. Lin, F.J. Tsai, J. Proteome Res. 17 (2018) 3997.
[46] L. Shi, C. Brunius, M. Lehtonen, S. Auriola, I.A. Bergdahl, O. Rolandsson, K. Hanhineva, R. Landberg, Diabetologia 61 (2018) 849.
[47] J. Lu, G. Xie, W. Jia, W. Jia, Front. Med. 7 (2013) 4.
[48] F. Xu, S. Tavintharan, C.F. Sum, K. Woon, S.C. Lim, C.N. Ong, J. Clin. Endocrinol. Metab. 98 (2013) E1060.
[49] J. Cobb, A. Eckhart, R. Perichon, J. Wulff, M. Mitchell, K.P. Adam, R. Wolfert, E. Button, K. Lawton, R. Elverson, B. Carr, M. Sinnott, E. Ferrannini, J Diabetes Sci Technol 9 (2015) 69.
[50] T.J. Wang, M.G. Larson, R.S. Vasan, S. Cheng, E.P. Rhee, E. McCabe, G.D. Lewis, C. S. Fox, P.F. Jacques, C. Fernandez, C.J. O'Donnell, S.A. Carr, V.K. Mootha, J. C. Florez, A. Souza, O. Melander, C.B. Clish, R.E. Gerszten, Nat. Med. 17 (2011) 448.
[51] S. Park, K.C. Sadanala, E.K. Kim, MOL CELLS 38 (2015) 587.